Development of Highly Homogenous Quantum Dot Micropillar Arrays for Optical Reservoir Computing

Tobias Heuser, Jan Große, Steffen Holzinger, Maximilian M. Sommer, and Stephan Reitzenstein

(Invited Paper)

***Abstract*—Neuromorphic computing has received considerable attention as promising alternatives to classical von Neumann computing architectures. An attractive concept in this field is reservoir computing which is based on coupled non-linear elements to enable for instance ultra-fast pattern recognition. We focus on the development of microlasers in a dense regular array for the implementation of photonic reservoir computing based on the diffractive coupling. The coupling relies on injection locking of microlasers and sets stringent requirements on the spectral homogeneity of the array, which needs to be on the order of the achievable locking range. We realize GaAs/AlGaAs micropillar arrays with InGaAs quantum dots as active medium. To achieve the high spectral homogeneity on the order of 100 μeV, as determined by injection locking experiments, the emission energy of each individual micropillar is adjusted to compensate for local inhomogeneities of order $\sim$1.3 meV in the underlying microcavity structure. The realized micropillar arrays have a spectral inhomogeneity as low as 190 μeV for an 8 $\times$ 8 array and down to 118 μeV for a 5 $\times$ 5 sub-array. The arrays have high potential to enable the implementation of powerful photonic reservoir computing, which can be extended to a reservoir of hundreds of microlasers in the future.**

***Index Terms*—Laser arrays, diameter tuning, injection locking, micropillars, neuromorphic computing, quantum dots.**

I. Introduction

NEUROMORPHIC computing dates back to the pioneering work by C. Mead [1] and has become a highly attractive alternative to von Neuman architectures in a period when Moore's law comes to an end [2]. Inspired by nature it sets out to mimic biological neural systems with high potential to outperform classical computing in complex tasks such as real-time learning and ultrafast image or pattern recognition via highly parallel architectures with multiple interactions [3]–[5]. An interesting and powerful implementation of neuromorphic computing is reservoir computing (RC) [6]–[9]. The underlying concept consists of a reservoir which maps input signals into a high-dimensional space followed by a readout signal which is formed by weighted connections of the reservoir. A particular advantage of RC is efficient learning via linear regression and classification.

RC can be implemented using different physical platforms, which can be categorized into electronic and photonic architectures. While electrical implementations of RC have the advantage of small footprint and compatibility with conventional electronics in possible hybrid concepts [10], [11], optical implementations profit from high scalability and high speed [12]. One appealing optical implementation of RC is based on diffractively coupled laser arrays [13], [14]. Here, the optical input signal is fed into an array of lasers which are coupled by external optics to form the reservoir, and the output signal is generated by a weighted sum of the laser's intensity. The whole system is trained by adjusting the individual coupling strengths between the lasers and by properly choosing the weighted sum at the output node. Once trained, such an implementation of RC can be operated at GHz speed and above. Here, the bandwidth is determined by the internal dynamics of the lasers acting as non-linear elements and the roundtrip time, on the order of nanoseconds, of the light signals in the external optics. Importantly, the implementation of RC via this concept relies on the efficient mutual coupling of the lasers in the array via injection locking. This in return sets stringent requirements on the optical properties of the laser array, which needs to show high spectral homogeneity. Here, deviations of the emission energy must not exceed the achievable injection locking range typically on the order of a few tens to a few hundreds of μeV.

Photonic RC has been implemented successfully and the concept has proven to be indeed very flexible, powerful and easy to train [15]. These early implementations include RC in small scale 5 $\times$ 5 vertical cavity surface emitting laser (VCSEL) arrays and a proof-of-principle demonstration of RC in a large-scale photonic recurrent neural network of up to 2025 diffractively coupled passive photonic nodes [8]. To take full advantage of photonic RC enabled by the diffractive coupling of active non-linear elements, it is necessary to improve the photonic hardware to maximize the number of involved lasers in the reservoir. This is not possible by simply extending the number of VCSELs in a 2D array because for a given size of the VCSEL and the related pitch on the order of 100 μm for the optics used with an effective coupling range of about 300 μm $\times$ 300 μm limits the

Manuscript received April 12, 2019; revised June 25, 2019; accepted June 27, 2019. Date of publication July 1, 2019; date of current version August 22, 2019. This work was supported in part by the European Research Council (ERC) under the European Union's Seventh Framework ERC Grant Agreement 615613 and in part by the Volkswagen Foundation via NeuroQNet. *(Corresponding author: Stephan Reitzenstein.)*

The authors are with the Institute of Solid State Physics, Technische Universität Berlin, 10623 Berlin, Germany (e-mail: tobias.heuser@tu-berlin.de; jan.grosse@tu-berlin.de; steffen.holzinger@tu-berlin.de; milosommer@hotmail.de; stephan.reitzenstein@physik.tu-berlin.de).

Color versions of one or more of the figures in this article are available online at http://ieeexplore.ieee.org.

Digital Object Identifier 10.1109/JSTQE.2019.2925968

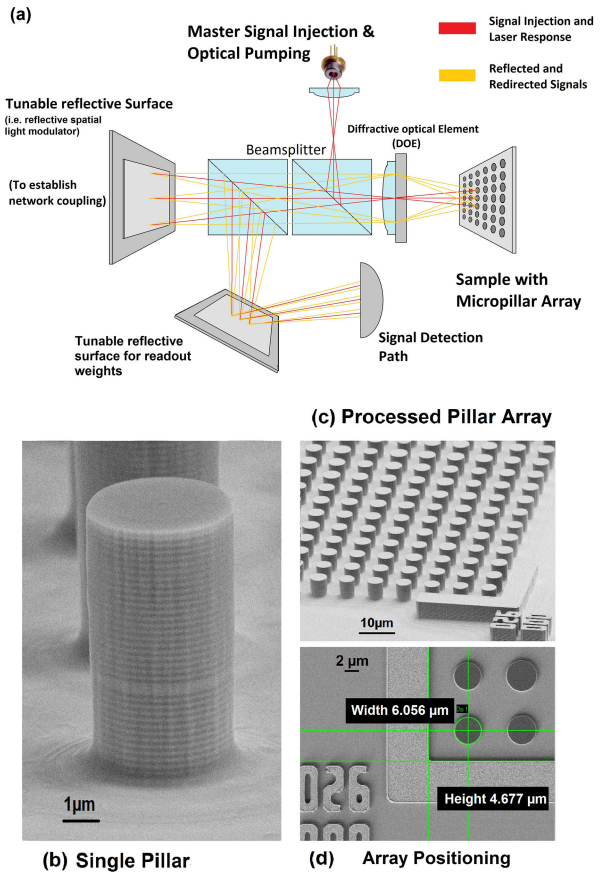

Fig. 1. (a) Scheme of the nanophotonic implementation of reservoir computing using a dense micropillar array, which is coupled by diffraction optics, adopted from Ref. [13], [14]. (b–d) SEM Images of a single micropillar (b) and micropillar arrays (c). In the fabrication process the pillar array is aligned with a target distance of 5 μm to marker structures with positioning accuracy better than 1 μm.

achievable reservoir dimension to a 9 $\times$ 9 array. Additionally, in conventional, commercially available VCSEL arrays, the emission wavelength of individual lasers usually differs in a range well beyond the available injection locking range and can hardly be compensated by injection-current induced wavelength tuning.

To boost the capabilities and computation power of photonic RC based on coupled laser arrays, we proposed to use dense homogeneous arrays of microlasers as indicated in Fig. 1(a). In this concept, the microlaser-array acts as nanophotonic hardware to enable photonic reservoir computing. In the envisaged concept, pillars in the array are diffractively coupled via a diffractive element in combination with a spatial light modulator (SLM) to adjust the individual coupling strengths. The reservoir is driven by optical pumping and the input signal is optically injected by two independent external lasers. Once trained via adjusting the readout weights at the second SLM, the system delivers the "calculated" output signal at a fast photodetector (signal detection). For more details we refer to Refs. [13]–[15]. Micro- and nanolasers have received enormous interest in recent years because they allow researchers to explore the limits of these optoelectronic devices, for instance with respect to size and threshold pump powers [16]. Interestingly, while arrays of coupled VCSELs have already been studied [17]–[20], coupling of nano- and microlasers is still at its infancy. In fact, such devices have been investigated almost exclusively as individual devices and mutual coupling of microlasers has only been realized and studied very recently [21].

One interesting type of microlasers is based on high-quality quantum dot (QD) micropillar cavities, which have enabled numerous studies and advances in the field of cavity-enhanced lasers [22]. Such QD-micropillar lasers with diameters typically in the 1 μm–5 μm range have comparatively small mode volumes and large cavity quality (Q) factors of several tens of thousands, which leads to high spontaneous emission coupling factors (β-factors) of up to about 60% and low threshold pump powers [23]. The latter is very beneficial to keep the power consumption of photonic RC based on large scale micropillar arrays at an acceptable level.

Compared to, e.g., laterally emitting whispering gallery mode microlasers, QD-micropillar lasers are very advantageous for our envisioned application in photonic RC because of the very directional axial emission normal to the sample surface. Moreover, due to their small diameters, pitches between neighboring devices of 10 μm and below can easily be achieved enabling the realization of dense microlaser arrays with 30 $\times$ 30 and more lasers within the available area of about 300 μm $\times$ 300 μm for diffractive photonic enabled RC [24]. To this end, because of their tight 3D optical mode confinement the emission energy of micropillar lasers depends characteristically on the diameter. This fact can be used to homogenize the emission energy of micropillar arrays by precisely adjusting the diameter of each individual micropillar in large scale arrays during the fabrication process as we presented in Ref. [24].

In this work we report on the realization and in-depth optical study of high quality QD-micropillar arrays for applications in photonic RC. The devices are realized by epitaxial growth using metal-organic chemical vapor deposition (MOCVD) and subsequent nano-processing by means of high-resolution electron beam lithography (EBL) in combination with reactive-ion etching. With respect to the optical properties of these devices we provide focus on the lasing properties of the microlasers and their response to external perturbations in terms of injection locking. Beyond that we refine the diameter-tuning concept for the fabrication of homogenous large-scale laser arrays by including also local optical variations of the underlying wafer material to the reach record high spectral homogeneity with a deviation of 190 μeV for an 8 $\times$ 8 micropillar array and a value of 118 μeV for a 5 $\times$ 5 micropillar array which compares well with an extrapolated and measured locking range of about 200 μeV and 80 μeV respectively.

II. Sample Technology

The sample design for the micropillar arrays is based on a vertical laser structure grown by means of MOCVD. The design consists of a central one-λ thick GaAs cavity sandwiched between the lower and upper distributed Bragg reflectors (DBR), which are composed of 27 and 23 λ/4-thick $Al_{90}Ga_{10}As$/GaAs pairs, respectively. To ensure sufficient gain for lasing operation, the central cavity includes an active medium composed of three layers of self-assembled Stranski-Krastanow InGaAs QDs with a density of about 1 $\times$ 10^{10} cm^{-2} each. Here, the main advantage

of using QDs (instead of quantum wells) is the rather large inhomogeneous broadening of the ensemble emission which in our case is about 50 nm on a planar sample. This facilitates spectral resonance between the cavity mode and the gain medium. Moreover, tight carrier confinement in QD allows us to reduce detrimental non-radiative surface recombination which could be an issue when using quantum wells as gain medium in small diameter micropillars.

To enable the diameter-tuning approach for the realization of homogeneous micropillar arrays, the corresponding sample material is pre-characterized regarding the x, y-position dependent resonance energy $E_0(x, y)$ of the planar cavity as described in detail in Section IV. Processing of micropillar arrays starts with depositing a 500 nm thick SiN-layer on the sample which acts as a hard mask in the final etching process. Then the sample is spin-coated by the "AZ nlof 2000" series negative-tone resist and the pillar cross-section is defined into the resist by EBL, after which the pillar pattern is transferred into the SiN layer by reactive ion etching (RIE) using a SF_6 plasma. The resulting circular shaped SiN etch masks feature steep edges which is the basis for the realization of micropillar cavities with smooth and vertical sidewalls using reactive ion etching (RIE) in an inductively coupled plasma containing Ar_2, Cl_2, and BCl_3. Fig. 1 shows scanning electron microscopy (SEM) images of a single micropillar with a diameter of 4 μm (panel (b)) and an array of micropillar cavities with a pitch of 8.3 μm (panel (c, d)). Finally, the sample is planarized with benzocyclobutene (BCB) to prevent oxidation of the Al containing layers of the DBRs and for mechanical stabilization. For this purpose, the BCB is spin-coated on the sample before curing and hardening it in an oven under N_2-atmosphere. The top facets of the micropillars are reopened in a RIE process using a CF_4/O_2 plasma, which also removes the remaining SiN of the hardmask, leading to a clean upper facet. Fig. 1(d) shows a zoom-in view of one corner of the micropillar array before etching and indicates its x-y alignment with respect to a marker structure. More details on the design and fabrication of QD-micropillars can be found in Ref. [25].

III. Lasing Characterization & Locking Range

In this section we address the optical properties of single QD-micropillars within an array to explore the general emission properties and the lasing behavior. Additionally, we present and discuss injection locking experiments which allow us to determine the locking range of the realized microlasers in master-slave configuration as an important figure of merit with respect to the spectral homogeneity of the dense micropillar arrays to be discussed in Section V. Please note that the purpose of this work is to optimize the optical properties of QD-microlasers arrays for future application in photonic reservoir computing. The implementation of the optical reservoir computing scheme described in Section I is beyond the scope of the present work.

The optical characterization of the planar wafer material and the dense micropillar arrays is performed by means of high-resolution micro-photoluminescence (μPL) spectroscopy. The sample is placed in a liquid He flow cryostat equipped with a motorized x-y-z stage to enable efficient mapping of the planar

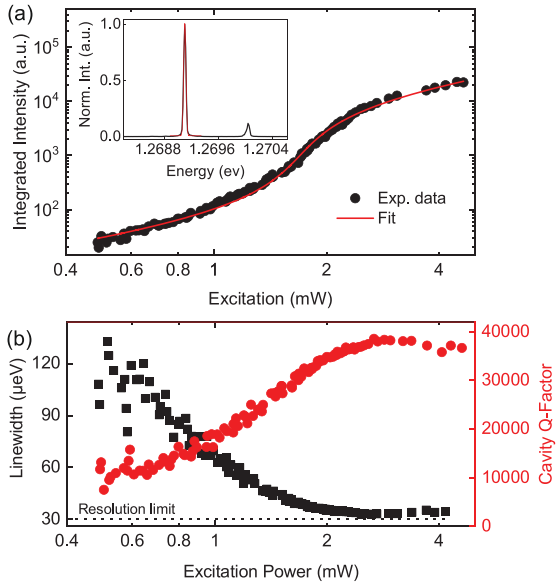

Fig. 2. Excitation power dependent emission properties of a 5 μm diameter pillar. (a) Input-output characteristics in double logarithmic scale. High-β laser action is identified by the characteristic s-shaped power dependence, which indicates the transition from spontaneous emission to lasing occurs at about 1.2 mW when a nonlinear increase of the emission intensity sets in as a signature of stimulated emission. A fit (red curve) to the experimental data (black bullets) yields a β-factor of 2%. Inset: Above threshold μPL spectrum at an excitation power of 3.4 mW. The Gaussian lineshape fit (red trace) yields an energy of the fundamental HE11 emission mode of 1.2691 eV. (b) Corresponding power dependent emission linewidth γ and Q-factor with $Q = E_{HE11}/\gamma$. The linewidth decreases due to the squeezing of saturation and because of increasing temporal coherence at high excitation powers and reaches the resolution limit of the spectrometer at an excitation power of about 2.5 mW.

sample and the processed micropillar arrays. The measurements are performed at 77 K, where the cooling is necessary to reduce non-radiative losses by thermal escape of carriers from the QDs with rather shallow carrier confinement. Individual pillars are optically driven with above bandgap excitation using solid-state lasers emitting at either 671 nm or 780 nm. The laser light is focused on the sample surface using a microscope objective with a numerical aperture (NA) of 0.4 and the emitted PL signal is collected by the same objective and detected via grating spectrometer with an attached charge-coupled device (CCD) camera with a spectral resolution of 30 μeV. In case of injection locking investigations, the CCD camera is replaced by a Fabry-Pérot interferometer (FPI) with a Si avalanche photon diode based single-photon counting module (SPCM), which has a free spectral range of about 7.5 GHz and a spectral resolution of 0.2 GHz.

Fig. 2 shows the excitation power dependent emission properties of a micropillar laser with a diameter of 5 μm and a (absorption limited) Q-factor of about 10.000 at low excitation power. The inset of panel (a) depicts an above-threshold μPL-spectrum recorded at an excitation power of 3.4 mW. The fundamental HE11 cavity mode is clearly identified and emits at an energy of $E_{HE11} = 1.2691$ eV, which is also the only mode having enough gain to reach the lasing threshold, so that the pillar effectively shows single-mode emission. Noteworthy, while for the given QD density of 10^{10} cm^{-2} a pillar of 5 μm diameter contains a total of about 6000 QDs in the three active layers, only a small

fraction of typically 10% of these emitters contribute efficiently to laser action because of the partial spectral and spatial overlap with the cavity mode [26], [27]. The excitation power dependent integrated intensity of the HE11 mode is plotted in panel (a) in double-logarithmic scale. Below threshold the intensity shows linear scaling, before laser oscillation sets in in the threshold region around 1.2 mW above which stimulated emission leads to a nonlinear increase of the output intensity. At even higher excitation powers linear scaling of the emission intensity is again observed. The smooth s-shaped transition between the two linear regions of the curve is nicely described by the theoretical curve (red trace) according to the solution of a rate equations model (Eq. (2) in Ref. [25]) which yields a β-factor of 2% (with $\zeta = 1.9$). This value is significantly larger than $10^{-4}-10^{-5}$ observed for standard VCSELs but smaller than 70% reported in Ref. [23], which is explained by the significantly smaller pillar diameter of 0.95 μm in that work and, thus, larger light-matter interaction. We like to mention that in general, increasing the β-factor reduces the threshold power [29] which is beneficial with respect to the energy efficiency of the envisioned application in neuromorphic computing. On the other hand, it can lead to partial injection locking [30] which can be compensated by high injection laser powers. Thus, in the implementation of RC one need to find a good balance between the two diametric effects for optimum energy efficiency.

The onset of laser action is confirmed by the corresponding power dependence of the emission linewidth presented in Fig. 2(b) along with the associated Q-factor. Starting from an absorption limited low-excitation, absorption limited value of about 60 μeV the linewidth decreases during the lasing transition until the resolution limit of 30 μeV is reached at an excitation power of about 2.5 mW. The Q-factor has a lower, absorption limited, bound of about 10.000 at low excitation powers and increases up to about 15.000 near threshold. This value is in good agreement with the theoretical prediction of 16.000 obtained by finite-element simulations for the used 27/23 DBR mirror design. For a direct comparison between theory and experiment we would need to identify the transparency pump power which is not feasible with the experimental techniques and data at hand.

Overall, the optical data presented in Fig. 2 shows that the fabricated cavities are performing as high-β microlasers with a clear transition to stimulated emission. As such, the microlasers fulfill the necessary condition for acting as nanophotonic nodes in the photonic RC implementation. Another crucial requirement to enable this target application is a suitable high coupling efficiency and locking range under optical injection. To explore this important feature for our microlasers, we performed injection locking experiments under variation of the locking strength. For this purpose, the emission of an external narrowband ($<$ 1 MHz linewidth) tunable laser (master) was injected into the fundamental mode of the micropillar (slave) under variation of the master-slave detuning. The microlaser is simultaneously pumped by a CW laser with an excitation power of 4.2 mW at 780 nm to ensure laser operation of the slave.

In the injection locking experiment, the slave laser oscillated at a fixed frequency (its solitary frequency) and the master laser was tuned continuously through spectral resonance with

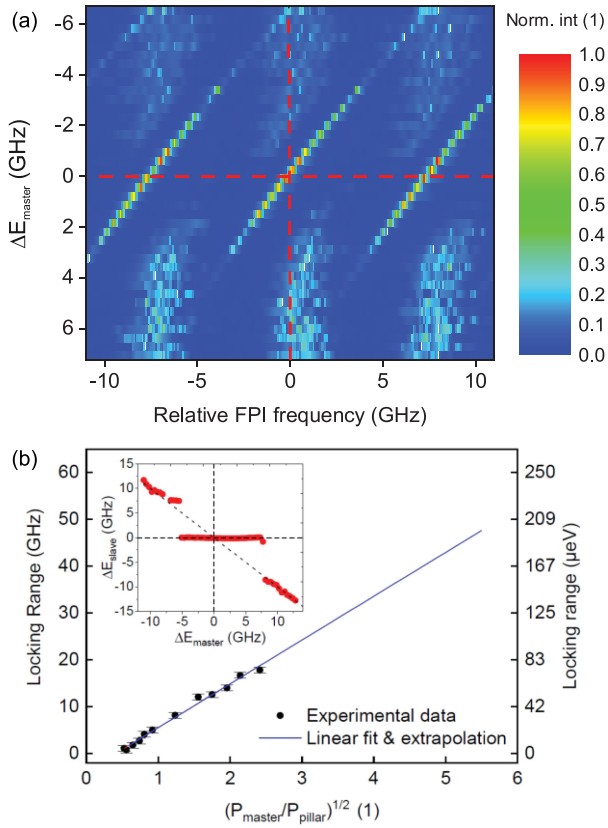

Fig. 3. Injection locking of a 5 μm QD-micropillar laser at varying injection strength. (a) 2D map showing the emission intensity as a function of the master-slave detuning ΔE_{master} and the relative FPI frequency for an injection power ratio of $P_{Master}/P_{Pillar} = 0.27$. The frequency extends over three free spectral ranges (7.5 GHz) of the FPI. Red dashed lines indicate the central locking feature. The narrow diagonal lines correspond to emission at the master laser frequency, while the broader vertically oriented emission features correspond to the slave microlaser. The microlaser clearly locks to the tunable external master laser in resonance for $\Delta E_{master} = \pm 0.5$ GHz and the locking range extends to about ± 2 GHz when emission at the master frequency gradually disappears. (b) Corresponding locking range (experimental and linear fit) as function of the injection strength in terms of $(P_{master}/P_{slave})^{1/2}$. Inset: Relative frequency of the microlaser (slave) as a function of the master-slave detuning extracted from the data for a power ratio $P_{Master}/P_{Pillar} = 2.43$.

the slave laser while detecting the joint emission using the high-resolution FPI. Fig. 3(a) presents the result of such an experiment in a 2D intensity map as a function of the master-slave detuning ΔE_{master} and the relative FPI frequency over three free spectral ranges of the FPI at an injection ratio of the master and slave power of $P_{Master}/P_{Pillar} = 0.27$. Close to zero detuning when both lasers are locked the narrow emission of the master laser dominates the spectrum for a detuning range of ± 0.5 GHz. Frequency locking is maintained in a transition region of about ± 2 GHz when the joint narrow emission signal strongly drops in intensity and gradually disappears.

To explore the injection strength dependence of the locking range, injection locking experiments were performed for multiple injection power ratios in the range of 0.13 to 5.84. The inset of Fig. 3(b) shows exemplarily the frequency locking curve for a power ratio of 2.43, which leads to a locking range of ± 5 GHz. The extracted locking ranges for all injection strengths are presented in Fig. 3(b). As expected, we observe a linear

increase of the measured locking range with $(P_{Master}/P_{Pillar})^{1/2}$, which is described by the common models for injection locking [31]–[34]. A maximum locking range of (17.8 ± 0.6) GHz ((73 ± 3) μeV) could be determined in the experimentally accessible injection power range.

We would like to note that this range was limited by the available effective master laser pump power (85 μW at the sample) and that by increasing the effective injection power the injection range can easily be extended as indicated by the linear fit to the experimental data and its extrapolation in Fig. 3(b). To estimate the required homogeneity, one has to divide the available injection power into each pillar in the array. Taking into account for example a master laser power of 500 mW and an array of 900 micropillars, each with an emission power of 10–20 μW, we estimate a required spectral homogeneity on the order of 200 μeV (∼50 GHz) based on the data extrapolated in Fig. 3(b) which the arrays have to fulfill to be usable for efficient diffractive coupling via injection locking. The corresponding injection power of 550 μW is still significantly lower than the threshold pump power of the micropillars shown in Fig. 2 so that we do not expect any thermal or non-linear effects to influence the extrapolated dependence of the available injection locking range.

IV. Diameter Tuning for Resonance Homogeneity

The fabrication of highly homogeneous large-scale micropillar arrays is a challenging task. This is mainly explained by the fact that the underlying planar microcavity sample material has spectral inhomogeneities related to the radial dependence of the resonance energy E_0. This feature is typical for epitaxially grown samples under rotation of the wafer, which usually leads to thinner layers of the DBRs towards the edge of the wafer. For the sample discussed in this work, we observe a thickness variation of about 2% (i.e., roughly 3 nm per DBR mirror pair) from the center to the edge of the wafer, which transforms to an overall resonance energy shift of 29 meV along the radius of the used 2 inch wafer. Additionally, local fluctuations of the layer thickness can occur due to non-ideal growth which also changes E_0. As can be seen in (1) below both effects directly affect the emission energy of the micropillar cavities.

Thus, in order to reach the high spectral homogeneity required for injection locking of the lasers in photonic RC, one must compensate for the spectral inhomogeneity of the underlying wafer material. In the best case, this is achieved by the nanofabrication process. In our fabrication concept, we improve the spectral homogeneity of the processed microlaser array by using the diameter dependence of the micropillars, which is a result of the lateral mode confinement. To enable this scheme, we first map the resonance energy of the planar microcavity in the specific wafer region by μPL spectroscopy, using the setup described in Section III. before processing micropillars with individually adjusted diameter. Here, E_0 is mapped with a maximum step-size corresponding to the pitch of the later pillar array. In this way, each pixel of the spectral map ideally includes the local energy E_0 at the position of a micropillar. Next, we calculate for each micropillar the required diameter d_c to compensate for the spectral inhomogeneity and to meet the target energy E_{HE11} with in the dense micropillar array via [34], [35]

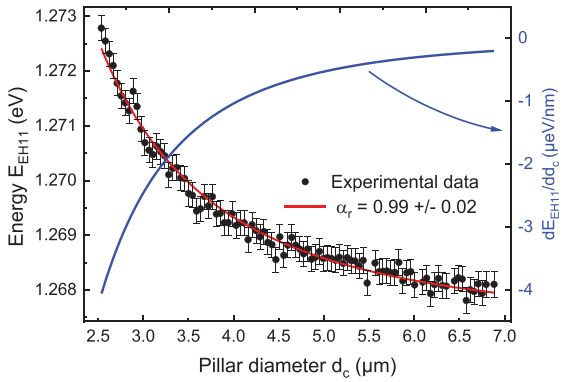

Fig. 4. Emission energy of the E_{EH11} pillar mode vs. pillar diameter d_c and its derivative (blue trace). A fit of the experimental data (black dots) according to (1) yields $\alpha_r = 0.99 \pm 0.02$ (red trace).

$$E_{HE11} = \sqrt{E_0^2 + \frac{\alpha_r \hbar^2 c^2}{\varepsilon_r} \frac{4x_{\varphi,r}^2}{d_c^2}}. \quad (1)$$

Equation (1) includes the effective dielectric constant of the cavity material ε_r, and the $n_{th,r}$ zero of the Bessel function $J_\varphi(x)\, x_{\varphi,r}$, which has a numeric value of 2.4048 for the considered HE_{11} mode. It also considers process dependent changes to the light confinement by the process dependent parameter α_r [24]. For instance, finite-element simulations of the mode confinement reveal that this parameter depends on the etching depth.

In practice it is crucial to determine α_r using a reference sample before fine adjustment of the pillar diameters in the final micropillar array using the same process and the same etching depth. Simulations in previous work [24] show a saturation of α_r close to 1 after etching of about 12 pairs of the bottom DBR for the used DBR design. Moreover, it is known that it is sufficient to etch only part of the lower DBR to achieve maximum Q-factors, while etching the full lower DBR can even be detrimental [36]. Therefore, the fabrication process was optimized for this etching depth. The $E_{EH11}(d_c)$ dependence of the reference sample is presented in Fig. 4. Fitting the experimental data by (1) yields $\alpha_r = 0.99 \pm 0.02$ for the present process parameters, showing that the saturation regime is reached. Based on the extracted α_r, one can now invert (1) to calculate the needed diameters to match the target E_{EH11} for given local E_0.

Fig. 4 reveals a total tuning range of about 5 meV in the investigated diameter region. However, the effective tuning range is limited to about 1 meV in the diameter region between 3.5 μm to 7.0 μm, in which the resulting mode energy is less sensitive to process related diameter variations [19]. Noteworthy, according to (1) and as seen in Fig. 4, the slope of $E_{EH11}(d_c)$ is higher in the small diameter limit which increases the available tuning range. However, in this diameter regime the emission energy is also more sensitive to diameter deviations caused by writing errors in the EBL process. Therefore, we usually perform diameter tuning in the large diameter range above 3.5 μm to achieve a good balance between large tuning range and insensitivity to

technological imperfections. For the micropillars discussed in this work we chose the diameter range to be between 4 μm and 5 μm, where absolute value of the slope $|d(E_{EH11}(d_c))/d(d_c)|$ is below 1 μeV/nm as can be seen in Fig. 4 (blue trace).

V. Marker Aligned Lithography of Arrays With Local Resonance Compensation

In the following we present details on fabrication of homogenous micropillar laser arrays using our diameter tuning concept. The present work builds upon previous results reported in Ref. [24] in which we presented that taking advantage of the diameter dependent optical confinement allows one to improve the spectral homogeneity of 30 $\times$ 30 micropillar arrays. In this proof-of-principle work the pillar diameters were calculated from a two-dimensional polynomial fit to the measured map of E_0 in the relevant unprocessed sample area and the later micropillar array was roughly aligned to the scanned area.

In this way, it was possible to increase the spectral homogeneity in terms of the standard deviation of the resonance energy distribution by 26% from about 350 μeV in the planar unprocessed sample to 260 μeV in the fabricated micropillar array. As we discuss in Ref. [24], the remaining inhomogeneity was attributed partially to local fluctuations of the resonance energy of the unprocessed wafer and to a smaller extend to technological imperfections in the EBL and etching process.

Here we tackle the issue of local wafer inhomogeneities and their impact on the fabricated micropillar arrays by a local mapping and the precise alignment of the pillar array to the scanned sample area. For this purpose, we first mapped the resonance energy E_0 of the unprocessed material by μPL scanning with 1 μm step size. A corresponding 2D luminescence map of a about 60 μm $\times$ 60 μm sample area is presented in Fig. 5(a). The sample region is in the center of the used wafer material in which the aforementioned radial dependence of E_0 (which would lead to a gradient of E_0 within the area) is negligible. However, we observe pronounced local fluctuation of E_0 in the range of 1.3 meV on a 1 μm to 10 μm scale, i.e., on the order the pillar diameter and the pillar pitch in the planned array of 8 $\times$ 8 micropillars whose later positions correspond to the crossing points of the dashed lines overlaid to the intensity map.

Considering the local variations of the resonance energy, a simple processing of pillars without diameter tuning would lead to a large spectral inhomogeneity of the micropillar array. To overcome this issue, we take the local resonance energy into account and calculate the required diameter for each of the 8 $\times$ 8 crossing points of the dashed lines in Fig. 5(a) according to Eq. (1) with a target energy of E_{HE11} = 1.27048 eV. Noteworthy, small scale variations of E_0 on a scale of the pillar diameter are considered by taking the average of 5 $\times$ 5 pixels (with 1 μm $\times$ 1 μm size) of the μPL map to determine the associated energy E_0 at each of the later pillar positions. Using these 8 $\times$ 8 energy values the corresponding pillar diameters were calculated and are plotted in Fig. 5(b). The calculated diameters lie in the range between 4.37 μm and 5.22 μm and the position of pillar with index (x, y) = (1, 1) corresponds for instance to (x, y) = (0, 0) in Fig. 5(b) and so on for the other

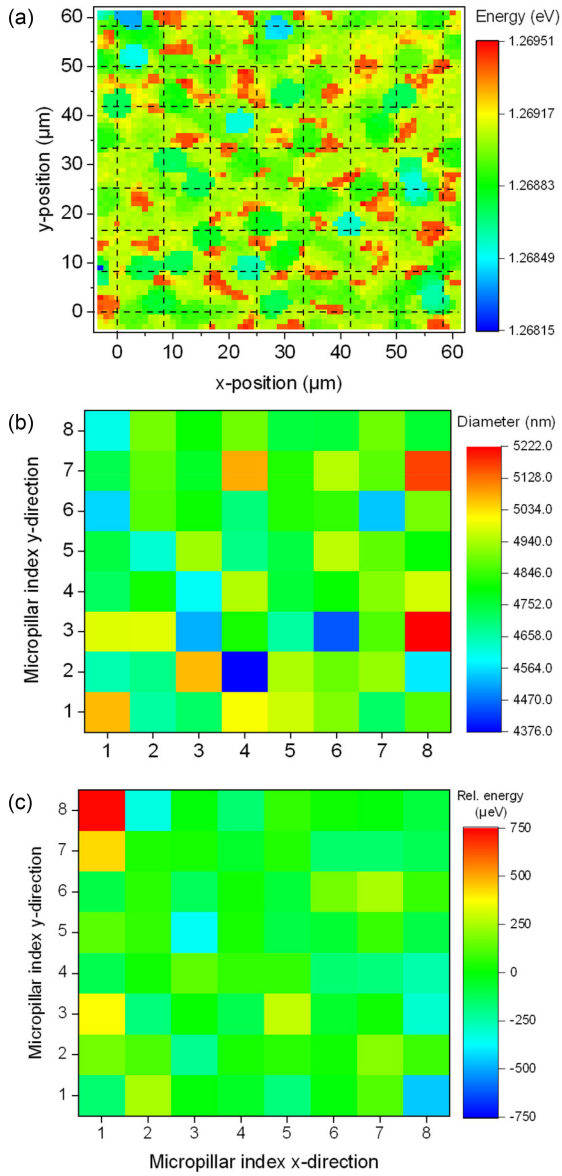

Fig. 5. (a) μPL scan of the resonance of the unprocessed planar laser structure with 1 μm resolution. The crossings of the dashed lines show the positions of the later fabricated pillar array. (b) Calculated diameter pattern which addresses the local energy fluctuations in (a) which were averaged over a diameter of 5 μm. (c) Relative emission energy of the HE11 mode of the fabricated micropillar array.

pillars. In the color coding it is nicely seen that the diameter of pillars at positions with large (small) E_0 are larger (smaller) than the average value. For instance, the calculated diameter of pillar (8, 3) with E_0 = 1.26926 eV is 5.222 nm (red color), while pillar (4, 2) has a diameter of 4.376 nm (blue color) and E_0 = 1.26874 eV.

Based on the calculated diameters the 8 $\times$ 8 pillar array was processed as described in Section II. Special care was taken to ensure a high alignment accuracy of the patterned arrays with respect to the pre-scanned positions to take full advantage of the local compensation of spectral homogeneity as described in the previous paragraphs. The resonance measurement of the finished micropillar array is now done in the same way as the

luminescence map of the planar sample by recording a μPL spectrum at each pillar position of the array. Fig. 5(c) presents the fitted energy of the fundamental mode (i.e., E_{HE11}) of the 8 × 8 micropillar array relative to the average energy of 1.27055 eV. This energy is only 70 μeV larger than the target energy of 1.27048 eV which can be explained by a small (constant) offset between the nominal and real diameter of the pillars of less than 100 nm. Importantly, the plot reveals that local diameter tuning leads to a highly homogeneous array in which most of the micropillars emit within a range of about 200 μeV relative to the average energy. Still, there are a few micropillars with a significantly larger deviation, such as pillar (1, 8). This issue is related to the fact that at a large gradient of E_0 is present at respective positions so that the emission energy of the pillar depends rather sensitively on the exact position and small alignment errors can lead to a large deviation from the target emission energy. Additional spectral deviations in the arrays can result from unavoidable writing errors of the EBL system. In our case, a standard deviation of the diameters on the order of 30 nm leads to spectral variations of 20–30 μeV in the used diameter range.

Finally, to evaluate the effect of diameter tuning in more detail we compare the spectral homogeneity of three 8 × 8 micropillar arrays realized without diameter tuning (array 1, fixed diameter $d_c = 5$ μm), with diameter tuning based on a polynomial fit of E_0 in the pre-scanned area (array 2), and on diameter tuning taking local fluctuations of E_0 into account (array 3). The three arrays were processed in parallel on the same chip to rule out wafer or process related effects on the spectral homogeneity. Corresponding 2D maps of the fundamental mode energy relative to the average energy of the pillars in the array are presented in Fig. 6(a)–(c) using the same color coding for a direct comparison. In case of array 1 with a standard deviation of E_{EH11} of 342 μeV only 20 pillars lie in the target range of about ±100 μeV (bright green) accessible via injection locking (see Fig. 3(b), and 9 pillars are outside the spectral range ±500 μeV (black). Array 2 shows already significantly improved optical properties with a standard deviation of 225 μeV and 26 pillars with emission in the ±100 μeV range and only three pillars outside the ±500 μeV window. Highest spectral homogeneity is achieved for array 3 with a standard deviation of 190 μeV, 33 pillars emitting in the ±100 μeV range and only one pillar outside the ±500 μeV window. Interestingly, only array 3 includes a larger 5 × 5 area (upper right corner, indicated by dashed lines) in which all pillars emit within a spectral range of ±300 μeV. Panel (d) presents a zoom-in μPL map of this area recorded with a step size of 1 μm. The standard deviation of this sub-array is 118 μeV and 23 out of 25 micropillars show emission within a ±300 μeV window.

Overall the present data clearly highlights the importance and potential of diameter tuning for achieving micropillar arrays with high spectral homogeneity. Most promising is the tuning approach which considers also local variations of the wafer's resonance energy. With a standard deviation down to 118 μeV in micropillar arrays the developed technology meets already the requirements of photonic RC based on the diffractive coupling of microlasers. Further developments could focus on the epitaxial growth of microcavity structures with improved homogeneity and on the optimized processing with better diameter control.

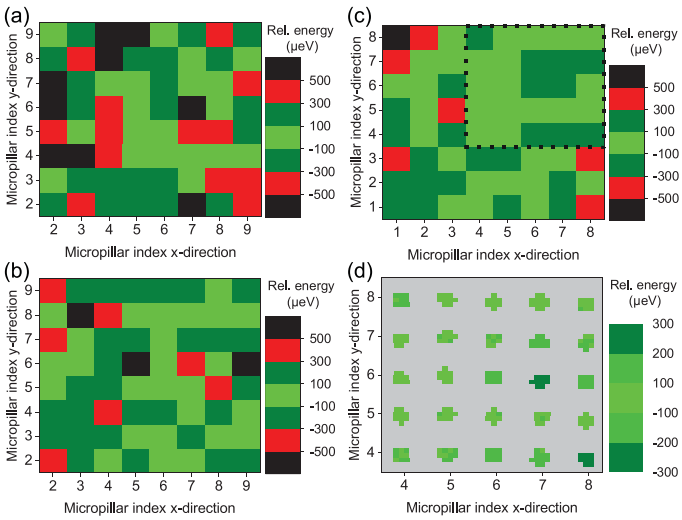

Fig. 6. Maps of E_{HE11} relative to the average energy for an uncompensated array (a), a compensated array by polynomially fitted resonances (b) and the locally compensated array (c) from Fig. 5. The local compensation increased the number usable pillars in the relevant energy window of 100 μeV from 20 (31%) to 33 pillars (51%) as compared to the uncompensated case, which also form more connected areas like the one marked in (c) that is shown in a detailed μm resolved scan in (d). We attribute the slight position dependence of E_{HE11} for some of the pillars in panel (d) to heating of the pillar which depends on the position of the laser spot on the upper facet of the micropillar.

VI. Summary

In summary, we developed a nanoprocessing platform for the realization of highly homogeneous arrays of optically pumped QD micropillar lasers for applications in photonic RC. The envisaged implementation of RC is based on the diffractive coupling in a dense array of vertically emitting microlasers. This application is enabled by the epitaxial growth of QD-microcavity structures and the subsequent nanoprocessing of regular micropillar cavity arrays using electron beam lithography and plasma etching. To meet the stringent requirements of photonic RC regarding the spectral homogeneity of the microlaser array, we developed an advanced diameter tuning technique in which we adjust the diameter of each individual micropillar in the fabrication process to compensate local variations of the resonance frequency, which occur in the underlying planar microresonator structure. Here, we take advantage of the tight light confinement and diameter dependent emission energy in the micropillar cavities, which allows us to control the emission energy by precisely setting the pillar diameter in the lithography process. In this way we achieve highly homogeneous micropillar laser arrays with a standard deviation as low as 190 μeV for an 8 × 8 pillar array and 118 μeV for an optimized 5 × 5 sub-array. These values compare well with extracted values of the injection locking range of about 200 μeV which give promise for a successful implementation of photonic reservoir computing based on the developed of nanophotonic hardware. Future work will focus on a further improving the spectral homogeneity by diameter tuning in combination with optimized epitaxial growth

to reduce the inhomogeneity of the planar microcavities and to enable large-scale RC in diffractively coupled arrays of hundreds of microlasers.

Acknowledgment

The authors would like to thank D. Brunner for helpful and inspiring discussions on the implementation and prospects of photonic reservoir computing.

References

[1] C. Mead, "Neuromorphic electronic systems," *Proc. IEEE*, vol. 78, no. 10, pp. 1629–1636, Oct. 1990, doi: 10.1109/5.58356.
[2] C. D. Schuman *et al.*, "A survey of neuromorphic computing and neural networks in hardware," May 2017, *arXiv:1705.06963*.
[3] H. Jaeger and H. Haas, "Harnessing nonlinearity: predicting chaotic systems and saving energy in wireless communication," *Science*, vol. 304, no. 5667, pp. 78–80, 2004, doi: 10.1126/science.1091277.
[4] D. V. Buonomano and W. Maas, "State-dependant computations: Spatiotemporal processing in cortical networks," *Nature Rev. Neurosci.*, vol. 10, no. 2, pp. 113–125, Feb. 2009, doi: 10.1038/nrn2558.
[5] J. P. Crutchfield, L. D. William, and S. Sudeshna, "Information processing in dynamical systems beyond the digital hegemony," *Chaos*, vol. 20, 2010, Art. no. 037101.
[6] K. Vandoorne *et al.*, "Toward optical signal processing using photonic reservoir computing," *Opt. Express*, vol. 16, no. 15, pp. 11182–11192, 2008, doi: 10.1364/OE.16.011182.
[7] L. Larger *et al.*, "Photonic information processing beyond Turing: An optoelectronic implementation of reservoir computing," *Opt. Express*, vol. 20, no. 3, pp. 3241–3249, 2012, doi: 10.1364/OE.20.003241.
[8] J. Bueno *et al.*, "Reinforcement learning in a large-scale photonic recurrent neural network," *Optica*, vol. 5, no. 6, pp. 756–760, 2018, doi: 10.1364/OPTICA.5.000756.
[9] M. S. Kulkarni and C. Teuscher, "Memristor-based reservoir computing," in *Proc. IEEE/ACM Int. Symp. Nanoscale Architectures*, Jul. 2012, pp. 226–232, doi: 10.1145/2765491.2765531.
[10] G. Indiveri, B. Linares-Barranco, R. Legenstein, G. Deligeorgis, and T. Prodromakis, "Integration of nanoscale memristor synapses in neuromorphic computing architectures," *Nanotechnology*, vol. 24, no. 38, Sep. 2013, Art. no. 384010, doi: 10.1088/0957-4484/24/38/384010.
[11] Y. Paquot *et al.*, "Optoelectronic reservoir computing," *Sci. Rep.*, vol. 2, Feb. 2012, Art. no. 287, doi: 10.1038/srep00287.
[12] F. Duport, B. Schneider, A. Smerieri, M. Haelterman, and S. Massar, "All-optical reservoir computing," *Opt. Express*, vol. 20, no. 20, pp. 22783–22795, 2012, doi: 10.1364/OE.20.022783.
[13] D. Brunner and I. Fischer, "Reconfigurable semiconductor laser networks based on diffractive coupling," *Opt. Lett.*, vol. 40, no. 16, pp. 3854–3857, 2015, doi: 10.1364/OL.40.003854.
[14] S. Maktoobi, L. Froehly, M. Jacquot, and D. Brunner, "Diffractive coupling for optical neural network," presented at the Nonlinear Photon., 2018, Paper. NpTh4G.4, doi: 10.1364/NP.2018.NpTh4G.4.
[15] G. Van der Sande, D. Brunner, and M. C. Soriano, "Advances in photonic reservoir computing," *Nanophotonics*, vol. 6, no. 3, pp. 561–576, May 2017, doi: 10.1515/nanoph-2016-0132.
[16] W. W. Chow and S. Reitzenstein, "Quantum-optical influences in optoelectronics-An introduction," *App. Phys. Rev.*, vol. 5, 2018, Art. no. 041302, doi: 10.1063/1.5045580.
[17] H. Li, T. L. Lucas, J. G. McInerney, M. W. Wright, and R. A. Morgan, "Injection locking dynamics of vertical cavity semiconductor lasers under conventional and phase conjugate injection," *IEEE J. Quantum Electron.*,vol. 32, no. 2, pp. 227–235, Feb. 1996.
[18] S. T. M. Fryslie, M. T. Johnson, and K. D. Choquette, "Coherence tuning in optically coupled phased vertical cavity laser arrays," *IEEE J. Quantum Electron.*, vol. 51, no. 11, Nov. 2015, Art. no. 2600206.
[19] K. Sayyah *et al.*, "Two-dimensional pseudo-random optical phased array based on tandem optical injection locking of vertical cavity surface emitting lasers," *Opt. Express*, vol. 23, no. 15, 2015, Art. no. 19405, doi: 10.1364/OE.23.019405.
[20] G. Hergenhan, B. Lücke, and U. Brauch, "Coherent coupling of vertical-cavity surface emitting laser arrays and efficient beam combining by diffractive optical elements: concept and experimental verification," *Appl. Opt.*, vol. 42, 2003, Art. no. 1667, doi: 10.1364/AO.42.001667.
[21] S. Kreinberg *et al.*, "Mutual coupling and synchronization of optically coupled quantum-dot micropillar lasers at ultra-low light levels," *Nature Commun.*, vol. 10, no. 1, Apr. 2019, Art. no. 1539, doi: 10.1038/s41467-019-09559-2.
[22] C. Gies and S. Reitzenstein, "Quantum dot micropillar lasers," *Semicond. Sci. Technol.*, vol. 34, no. 7, Jun. 2019, Art. no. 073001, doi: 10.1088/1361-6641/ab1551.
[23] M. Lermer *et al.*, "High b lasing in micropillar cavities with adiabatic layer design," *Appl. Phys. Lett.*, vol. 102, no. 5, 2013, Art. no. 052114, doi: 10.1063/1.4791563.
[24] T. Heuser, J. Große, A. Kaganskiy, D. Brunner, and S. Reitzenstein, "Fabrication of dence diameter-tuned quantum dot micropillar arrays for applications in photonic information processing," *APL Photon.*, vol. 3, 2018, Art. no. 116103, doi: 10.1063/1.5050669.
[25] S. Reitzenstein and A. Forchel, "Quantum dot micropillars," *J. Phys. D, Appl. Phys.*, vol. 43, 2010, Art. no. 033001, doi: 10.1088/0022-3727/43/3/033001.
[26] S. Reitzenstein *et al.*, "Lasing in high-Q quantum-dot micropillar cavities," *App. Phys. Lett.*, vol. 89, 2006, Art. no. 051107, doi: 10.1063/1.2266231.
[27] S. Kreinberg *et al.*, "Emission from quantum-dot high-β microcavities: Transition from spontaneous emission to lasing and effects of superradiant emitter coupling," *Light: Sci. Appl.*, vol. 6, 2017, Art. no. e17030, doi: 10.1038/lsa.2017.30.
[28] S. Reitzenstein *et al.*, "Single quantum dot controlled lasing effects in high-Q micropillar cavities," *Opt. Express*, vol. 16, no. 7, pp. 4848–4857, 2008, doi: 10.1364/OE.16.004848.
[29] Y. Yamamoto, S. Machida, and G. Björk, "Microcavity semiconductor laser with enhanced spontaneous emission," *Phys. Rev. A*, vol. 44, 1991, Art. no. 657, doi: 10.1103/PhysRevA.44.657.
[30] E. Schlottmann *et al.*, "Injection locking of quntum dot microlasers operating in the few photon regieme," *Phys. Rev. Appl.*, vol. 6, 2016, Art. no. 044023, doi: 10.1103/PhysRevApplied.6.044023.
[31] T. Erneux and P. Glorieux, "Optically injected semiconductor lasers," in *Laser Dynamics*, 1st ed. Cambridge, U.K.: Cambridge Univ. Press, 2010, pp. 213–237
[32] A. E. Siegman, "Laser injection locking," in *Lasers*, 1st ed. Mill Valley, CA, USA: University Science Books, 1986, pp. 1130–1162.
[33] R. Adler, "A study of locking phenomena in oscillators," *Proc. IRE*, vol. 34, no. 6, pp. 351–357, Jun. 1946, doi: 10.1109/JRPROC.1946.229930.
[34] T. Gutbrod *et al.*, "Angle dependence of the spontaneous emission from confined optical modes in photonic dots," *Phys. Rev. B.*, vol. 59, no. 3, 1999, Art. no. 2223, doi: 10.1103/PhysRevB.59.2223.
[35] G. Panzarini and L. C. Andreani, "Quantum theory of exciton polaritons in cylindrical semiconductor microcavities," *Phys. Rev. B.*, vol. 60, no. 24, 1999, Art. no. 16799, doi: 10.1103/PhysRevB.60.16799.
[36] N. Gregersen *et al.*, "Numerical and experimental study of the Q factor of high-Q micropillar cavities," *IEEE J. Quantum Electron.*, vol. 46, no. 10, pp. 1470–1483, Oct. 2010, doi: 10.1109/JQE.2010.2052095.

Tobias Heuser was born in Berlin, Germany, in 1990. He started his studies in physics in 2009 from the Free University of Berlin, Berlin, Germany and received the B.Sc. degree in 2012, the M.Sc. degree from the TU Berlin, Berlin, Germany, in 2015 already in the group of Prof. Reitzenstein working on single-photon sources based on circular Bragg-grating cavities. He is currently working toward the Ph.D. degree by developing vertical laser structures for applications in modern neuro-inspired computing concepts. His research in the field of nanophotonic devices. Since 2009, he has been a member of the German Physical Society.

Jan Große was born in Neubrandenburg, Germany, in 1987. He received the B.S. and M.S. degrees in physics from Technische Universität Berlin, Berlin, Germany, in 2013 and 2016, respectively, in the field of surface science. Since 2016, he has been working toward the Ph.D. degree with the Institut für Festkörperphysik, TU Berlin, where he is working with the MOCVD Department. Since 2006, he has been a member of the German Physical Society.

Steffen Holzinger was born in Karlstadt, Bavaria, Germany, in 1987. He received the B.S. and M.S. degrees in nanostructure technology from the Julius-Maximilians-Univerität Würzburg, Würzburg, Germany, in 2011 and 2014, respectively. He is currently working toward the Ph.D. degree in physics with Technische Universität Berlin, Berlin, Germany. His research interest includes the non-linear dynamics feedback-coupled and injection-locked quantum-dot microlasers in the limit of cavity quantum electrodynamics. He is a member of the German Physical Society.

Maximilian M. Sommer was born in Berlin, Germany, on March 1992. He received the B. Sc. degree in physics from the Technische University Berlin, Berlin, Germany, in 2016. He is currently working toward the M. Sc. degree focusing on feedback-coupled and injection-locked quantum dot micropillar lasers in the regime of ultra-low light levels.

Stephan Reitzenstein received the Diploma and Ph.D. degree (*summa cum laude*) from the University of Würzburg, Würzburg, Germany, in 2000 and 2005, respectively, both in physics. In 2010, he habilitated with studies regarding optical properties of low dimensional semiconductor systems. Since September 2011, he has been a Full Professor with the Technical University of Berlin, Germany and holds the Chair of Optoelectronics and Quantum Devices. In 2014, he received a prestigious ERC Consolidator Grant on the external quantum control of nanophotonics systems. Since January 2016, he has been the Director of the Center of Nanophotonics with the TU Berlin. His current research interests are in the area of nanoelectronics and quantum optics in semiconductor nanostructures. He is a member of the German Physical Society where he is currently the spokesman of the semiconductor division.